

Spontaneous Production of Ultrastable Reactive Oxygen Species on Titanium Oxide Surfaces Modified with Organic Ligands

Ida Ritacco, Claudio Imparato, Laura Falivene, Luigi Cavallo, Alessandra Magistrato, Lucia Caporaso,* Matteo Farnesi Camellone,* and Antonio Aronne*

The spontaneous formation and long-term surface stabilization of superoxide radicals are observed on specific TiO₂ hybrid materials in which titanium is coordinated to an organic ligand. Here the rationale for this uncommon phenomenon is investigated by a synergistic theoretical and experimental approach involving density functional theory (DFT) calculations and spectroscopic techniques. Stoichiometric and reduced anatase (101) surfaces modified with acetylacetone, dibenzoylmethane, and catechol are comparatively examined. These results reveal that the interaction between organic ligands and adsorbed O₂ molecules improves when O vacancies are present on the external layer of the surface, promoting O₂ reduction. The electronic features of the ligand play a pivotal role for both an effective electronic interaction with the surface and the stabilization of the generated reactive oxygen species. These results agree with experimental data showing that sol–gel-derived Ti-diketonate hybrid oxides spontaneously produce very persistent superoxide radicals under ambient conditions, thus holding a high intrinsic oxidative activity.

1. Introduction

In recent decades, TiO₂ surfaces have assumed a role of fundamental importance in the environmental and health-care fields for pollutants' degradation and disinfection. In fact, following a proper activation treatment, usually by UV irradiation (photocatalysis), the electron–hole pairs trapped on these surfaces react with the adsorbed acceptor (oxygen) and donor (water) molecules forming highly reactive oxygen species (ROS) that are involved in the degradation of contaminants adsorbed on the surface.^[1–3] Particularly, the formation of the hydroxyl radical (·OH) seems to be favored on anatase TiO₂ while that of the superoxide anion radical (O₂^{·−}) on rutile TiO₂.^[3–5] The different photoinduced reactivities observed for these polymorphs can be related to the different modifica-

tions of their electronic structures occurring during the activation procedure.^[6]

Controlling the formation of ROS and their stabilization on solid surfaces is extremely attractive since these species not only are crucial for removing contaminants from water or atmosphere, but also hold a great potential for selective organic conversions,^[1,7] inactivation of bacteria and viruses,^[8,9] and for anticancer photodynamic therapy.^[10–12]


As such, there is a huge interest to extend the TiO₂ photoresponsivity to visible light and to explore and assess the parameters that induce the increase of ROS lifetime. Both scopes can be addressed by chemical modifications of the oxide surface. The adsorption of suitable organic molecules has been proposed as a versatile photosensitization strategy, alternative to doping^[13,14] and to the formation of heterojunctions with other semiconductors or carbon-based materials.^[15,16] Two main sensitization mechanisms have been described: in the first, the absorption of visible light by a dye molecule causes a highest occupied molecular orbital (HOMO)–lowest unoccupied molecular orbital (LUMO) transition, followed by electron injection into the conduction band (CB); in the second, a direct electron transfer from the ground state of the sensitizer into the CB occurs, without involving any excited state of the molecule (ligand-to-metal charge transfer, LMCT).^[16–18] Among the small organic molecules that are able to induce LMCT when coupled

Dr. I. Ritacco, Dr. L. Falivene, Prof. L. Caporaso
Dipartimento di Chimica e Biologia
Università degli Studi di Salerno
via Giovanni Paolo II 132, Fisciano, Salerno 84084, Italy
E-mail: lcaporaso@unisa.it

Dr. C. Imparato, Prof. A. Aronne
Dipartimento di Ingegneria Chimica
dei Materiali e della Produzione Industriale
Università di Napoli Federico II, P.le Tecchio 80, Napoli 80125, Italy
E-mail: anaronne@unina.it

Prof. L. Cavallo
KAUST Catalysis Center (KCC)
King Abdullah University of Science and Technology
Thuwal 23955-6900, Saudi Arabia

Dr. A. Magistrato, Dr. M. Farnesi Camellone
CNR-IOM
Consiglio Nazionale delle Ricerche—Istituto Officina dei Materiali
c/o SISSA, Trieste 34136, Italy
E-mail: farnesi@iom.cnr.it

 The ORCID identification number(s) for the author(s) of this article can be found under <https://doi.org/10.1002/admi.202100629>.

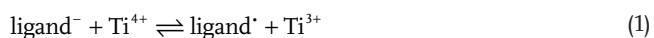
© 2021 The Authors. Advanced Materials Interfaces published by Wiley-VCH GmbH. This is an open access article under the terms of the Creative Commons Attribution-NonCommercial-NoDerivs License, which permits use and distribution in any medium, provided the original work is properly cited, the use is non-commercial and no modifications or adaptations are made.

DOI: 10.1002/admi.202100629

with TiO₂, enediols (catechol and its derivatives), phenols, carboxylic acids and diketones have been investigated.^[17–22]

The molecular structure of a ligand determines its binding mode to the metal and the energy levels of the frontier orbitals, which, in turn, affect the electronic coupling and the efficiency of the charge injection, separation, and recombination (back-electron transfer). For example, the different strength of LMCT complexes formed with Ti⁴⁺ by catechol compared to acetylacetonone or salicylic acid is associated with a variable degree of charge delocalization over the oxide particle.^[20] Depending on the type of interaction, differences in the mechanisms of ROS production can be expected.

The electron-transfer equilibrium processes leading to the formation of ROS on sensitized TiO₂ can be described according to Equations (1)–(4)



or



It should be noted that this is a simplified illustration, since an electron injected by the ligand may localize on either a Ti atom (as Ti³⁺) or another trap site (e.g., an oxygen vacancy), or may be rather delocalized on the CB. Moreover, surface defects, in particular, the differently charged oxygen vacancies (VO[•], VO⁺, VO^{••-}, VO^{•••2-}) found in metal oxides,^[23,24] also play a key role in the interaction with adsorbed molecules, including O₂ or H₂O.^[25,26] Therefore, Ti³⁺ is not necessarily entailed in electron trapping or can be transiently involved. The reactions giving O₂^{•-} can be described in different ways, as, for example, by Equations (5) and (6)



These oxygen radicals are highly reactive, showing very short lifetimes in water solution (in the order of seconds for O₂^{•-} and much lower for $\cdot\text{OH}$ ^[3,27]), and their stabilization on the TiO₂ surface is a tough challenge. Previous studies reported an increased lifetime of O₂^{•-} only under particular conditions in aqueous suspensions,^[27] while harsh pretreatments such as vacuum annealing^[25] or the use of radical initiators such as H₂O₂ in the synthesis procedure^[28] are still required in air.

In this scenario, some of us recently put on the stage a simple sol-gel route to obtain TiO₂-acetylacetonate (TiO₂-*acac*) and ZrO₂-acetylacetonate (ZrO₂-*acac*) hybrid materials (dried at low temperature), on whose surface O₂^{•-} radicals are spontaneously generated and stably adsorbed owing to the presence of *acac* ligands.^[29,30] In case of ZrO₂-*acac*, density functional theory (DFT) calculations showed that the *acac* ligand significantly lowers the formation energy of oxygen vacancies and the adsorption energy of O₂, driving its reduction to superoxide ion.^[31] Both ZrO₂-*acac* and TiO₂-*acac* gel-derived materials have shown remarkable catalytic activity in the degradation of model organic

pollutants without any need of light irradiation.^[21,29,30,32,33] These unusual catalytic performances, driven by the exceptional persistence (up to 3 years in air at room temperature) of O₂^{•-} on the surface of these amorphous materials,^[32] open a new perspective in the field of advanced oxidation processes (AOP) for the decontamination of polluted wastewaters.

A detailed understanding of this peculiar behavior and the possible regeneration of the superoxide radicals by exposition to air/water remains elusive, although it is expected that the features of the Ti⁴⁺-*acac* LMCT complex and the defective structure of the oxide surface play a key role in the process.

To clarify the influence of the electronic parameters involved in the charge-transfer process on the stabilization of O₂^{•-} on the surface of the hybrid TiO₂-ligand materials, in this work an extensive computational study was performed for both stoichiometric and O-defective anatase TiO₂ (101) surfaces, considering three different organic ligands: 2,4-pentanedione (acetylacetonone, *Hacac*), 1,3-diphenyl-1,3-propanedione (dibenzoylmethane, *Hdbm*), and 1,2-dihydroxybenzene (catechol, *H₂cat*). Complementarily, the results of DFT calculations were compared with the structural, optical, and electronic features of the corresponding systems synthesized by the sol-gel procedure.

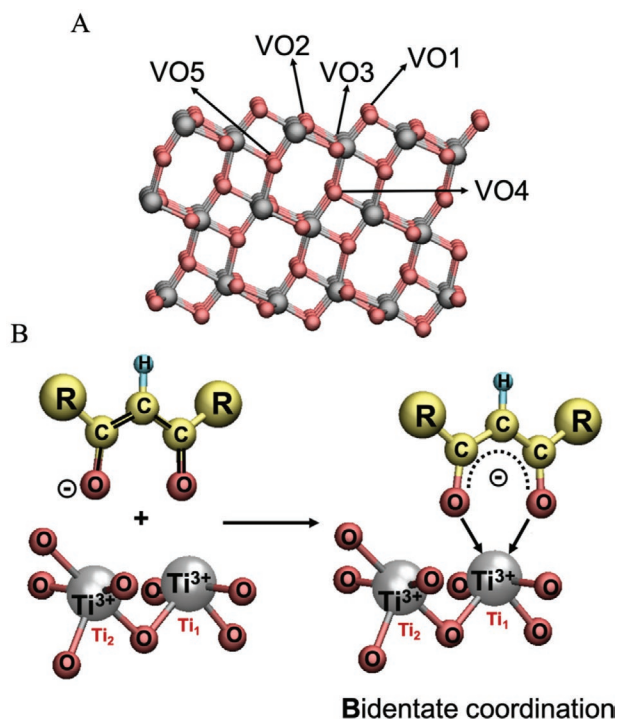
Like *Hacac*, *Hdbm* is a β-diketone, whose tautomeric equilibrium is completely shifted toward the enol form owing to the presence of two phenyl groups that, due to conjugation, stabilize even further the ligand's unpaired electron.^[34,35] On the other hand, the higher charge-transfer ability of *H₂cat* ligand as compared to *Hacac* and *Hdbm* helps in assessing the role of the interfacial charge-transfer properties on the formation and stabilization of O₂^{•-}.

2. Results and Discussion

2.1. Coordination of *acac* and *dbm* on Anatase TiO₂ (101) Surface Containing O Atom Defects

DFT calculations have been performed to investigate the structural and electronic properties of TiO₂-*acac* and TiO₂-dibenzoylmethanate (TiO₂-*dbm*) hybrid gel-derived materials. A detailed analysis of the projected density of state (PDOS), spin density, and Bader charges on systems consisting of a reduced anatase (ATiO₂) (101) surface bare and coordinated to ligands has been carried out. The corresponding results for the stoichiometric surfaces are reported in Section S1 of the Supporting Information for clarity and readability of the manuscript.

The local disorder, typical of amorphous hybrid metal oxides (e.g., TiO₂ or ZrO₂) synthesized by sol-gel,^[29,36] has been modeled by appropriately removing oxygen atoms from the stoichiometric TiO₂ (101) anatase surfaces, and different kinds of vacancies have been considered in order to identify the most stable sites. Namely, we have taken into account surface and subsurface O vacancies (**Scheme 1A**). The O vacancy labeled VO1 is obtained by removing a two-coordinated surface O2c atom, resulting in two surface-unsaturated Ti atoms, one tetracoordinate, Ti4c, and one pentacoordinate, Ti5c. These are hereafter denoted as **Ti1** and **Ti2**, respectively (see **Scheme 1B**). Conversely, the VO2–VO5 vacancies are obtained by removing a surface (VO2, VO3) or a subsurface (VO4, VO5) three-coordinated O3c atom, resulting in two Ti4c and one Ti5c for VO2, two Ti5c and



Scheme 1. A) Different surface and subsurface vacancy sites of ATiO_2 and B) acac/dbm-VO1 surface interaction. Ti, C, H, and O atoms are represented in ball and sticks and depicted in gray, yellow, cyan, and red, respectively.

one Ti4c for VO3 , three Ti5c for VO4 , and one Ti4c and two Ti5c for VO5 . The removal of one oxygen atom leaves an excess of two electrons within the surface that localize on the d orbitals of the Ti close to the vacancy, generating Ti^{3+} ,^[37] in agreement with the spin density plots reported in the Supporting Information.

As a result, the formation energies ($E_{\text{FORM}(\text{VO})}$) evaluated for the different O vacancies are 3.12 eV (VO1), 3.36 eV (VO5), 3.74 eV (VO4), and 4.28 eV (VO2 and VO3).

The VO1 surface is the most favorable one showing the lowest O vacancy formation energy, in agreement with previous studies.^[38] Therefore, in the following, we will focus only on the interaction of ligands with the defective anatase TiO_2 (101) surface in the presence of the VO1 surface vacancy.

Hacac and Hdbm deprotonate upon adsorption on ATiO_2 surface and in our model the resulting protons H^+ are put on O2c (bicoordinated O) atoms of the bottom layer of the surface far from the ligands in order to simulate the experimental sol-gel derived materials (see Section S4 of the Supporting Information). Furthermore, both molecules in enolate form adopt a bidentate coordination mode (B)^[29,31,36] with the two O atoms bonded to the under-coordinated Ti4c (Ti1) surface site close to the VO1 O vacancy. As a result, both ligands restore a hexa-coordinated configuration of the Ti1 atom (see Scheme 1). The optimized geometries (for more details, see Figure S5 in the Supporting Information) and the corresponding interaction energies (E_{int} , eV) for acac and dbm , equal to -2.58 and -2.73 eV, respectively (Figure 1A,B) indicate that the presence of a surface O vacancy, like VO1 , favors the bidentate (B) coordination over the bidentate bridge (BB) one (see Section S1 of the Supporting Information) and increases the stabilization of the adsorbed ligands.

Notably, in spite of the presence on the surface of the two excess electrons derived from the formation of the VO1 O vacancy, the computed variation of Bader charge, calculated as the difference between the charges of the ligand atoms in free and surface-bound forms (Δq ; Table S4, Supporting Information), suggests that additional charge migrates from the organic molecules to the surface. This is also confirmed by inspection of the bonding charge analysis (Figure S6, Supporting Information). The intensities of these charge transfers are very close to each other for both ligands (about 0.3 eV), in agreement with the similar E_{int} calculated (see Figure 1).

The PDOS plots of the lowest energy configurations with acac and dbm ligands coordinated to the anatase TiO_2 (101) surface in the presence of VO1 O vacancy are displayed in Figure 1A',B'. In both cases the valence bands (VB) have mainly O 2s and 2p characters and the CB display a Ti 3d character. The computed bandgap is 2.70 eV for both ligands, in agreement with the experimental values reported in the following. This value is similar to that of the analogous stoichiometric systems (Figure S4, Supporting Information) but smaller than the pure anatase (experimental gap of 3.2 eV^[21,39] and theoretical gap of 3.0 eV), suggesting that the presence of organic ligands contributes to reduce the TiO_2 surface bandgap.

The presence of the VO1 O vacancy leads to the appearance of distinct filled states (red peaks) in the TiO_2 bandgap, whose projection onto two specific Ti sites fully accounts for the entire peak integral area even in the presence of the two ligands (Figure 1A',B'). Indeed, it is well known that the removal of an O atom from TiO_2 gives rise to an excess of two electrons and the subsequent appearance of electronic states within the bandgap. Although these two electrons can, in principle, be localized on any Ti atom, they are believed to preferentially occupy Ti 3d orbitals of Ti atoms adjacent to the vacancy, formally creating Ti^{3+} sites.^[37]

The spin densities of the two systems, namely the reduced anatase TiO_2 (101) surface with coordinated acac and dbm , are depicted in Figure 1A'',B'', respectively. In both cases two reduced surface Ti^{3+} species are present (red densities).

2.2. Adsorption of O_2 Molecules on O-Defective Anatase TiO_2 (101) Surface Bare and Coordinated with acac and dbm

The role played by the ligands in the formation and stabilization of ROS on the reduced anatase surfaces has been addressed by calculating the interaction between O_2 molecules and the reduced ATiO_2 (101) surface bare and in the presence of coordinated acac and dbm molecules. The adsorption of a single O_2 molecule ("low oxygen coverage") and of two O_2 molecules ("high oxygen coverage"), which better reproduce the experimental conditions, has been considered^[40] (see Figure 2 and Table 1 for the VO1 surfaces. The same calculations performed for the stoichiometric surface are reported in Section S2 of the Supporting Information).

Figure 2 shows the optimized geometries with the corresponding adsorption energies (E_{ads}) with one and two O_2 molecules adsorbed on the surface.^[40,41] In agreement with other theoretical and experimental studies,^[40,42,43] our calculations suggest that the presence of an excess of charge on ATiO_2

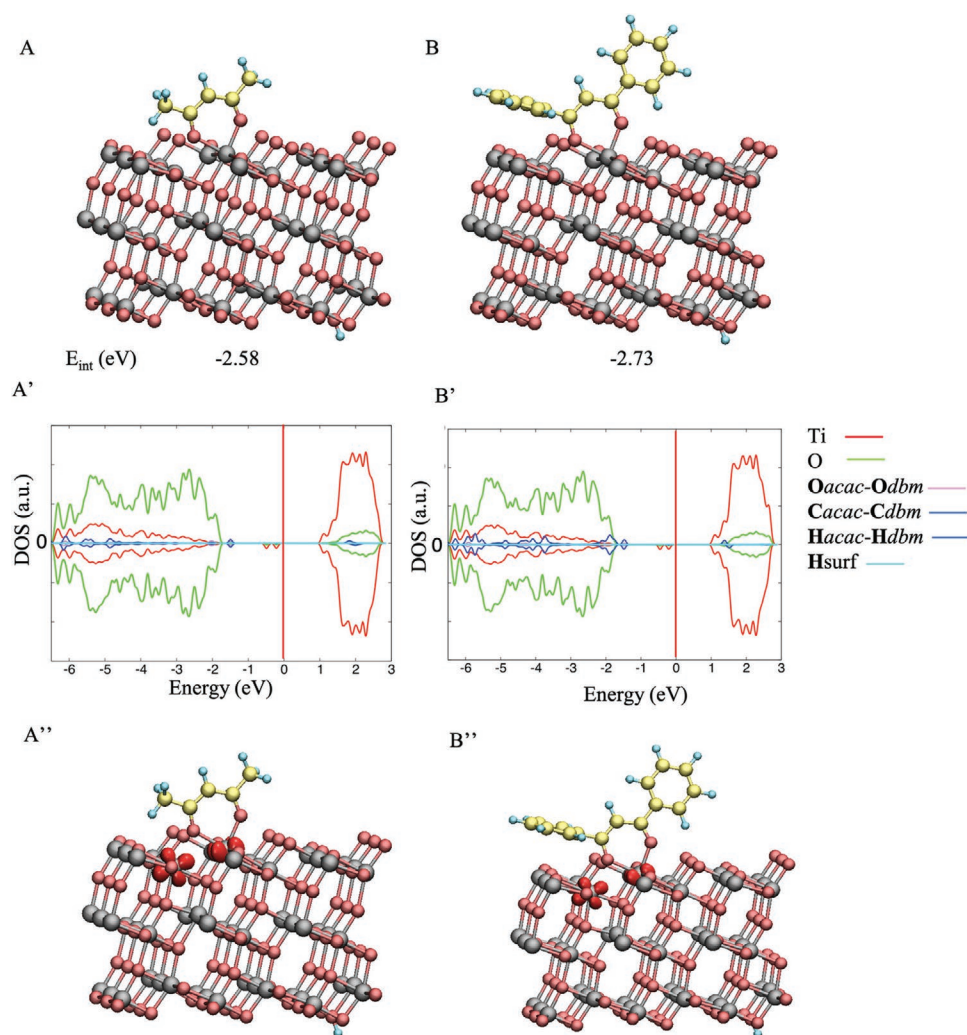


Figure 1. Optimized structures of the interaction of A) *acac* and B) *dbm* with the ATiO_2 (101) surface containing oxygen vacancy VO1 with the corresponding E_{int} (eV). Ti, C, H, and O atoms are represented in ball and sticks and depicted in gray, yellow, cyan, and red, respectively. A', B') PDOS and A'', B'') spin density plots for *acac/dbm*-VO1 systems, respectively. The state of titanium (Ti) and oxygen (O) surface atoms, oxygen (*Oacac*, *Odbm*), carbon (*Cacac*, *Cdbm*), and hydrogen (*Hacac*, *Hdbm*) ligand atoms, surface hydrogen (*Hsurf*) are represented in red, green, pink, blue, and cyan, respectively. On the DOS (a.u.) axis, the values above and below 0 a.u. indicate the electrons with spin up and spin down, respectively. The Fermi energy level is represented with a red line at 0 eV.

(101) surfaces is required to form and stabilize superoxide and peroxide anions. On the stoichiometric ATiO_2 surface, an O_2 molecule binds very weakly, with an adsorption energy of -0.06 eV (see Section S2 of the Supporting Information), and no charge is transferred from the support to the O_2 molecule. Instead, on the reduced surface, where a charge excess left by the O vacancy is present, O_2 binds more strongly to the surface (see Figure 2A), with an adsorption energy of -0.61 eV. Here, the charge is transferred from the surface to the adsorbed O_2 that turns into a superoxide radical anion.

Interestingly, the presence of *acac* and *dbm* molecules on the reduced TiO_2 (101) surface increases the interaction of O_2 species with the substrate lowering the adsorption energy of O_2 that becomes -0.99 – -0.94 eV at low oxygen coverage and -1.34 – -1.38 eV at high oxygen coverage (see Table 1).^[40,44]

The adsorption of molecular O_2 on the surface is expected to induce charge rearrangement and trigger a change in the

electronic properties of the surface and the binding molecules (O_2 and ligand).

To dissect the charge rearrangement induced on the surface by O_2 and ligands, we have analyzed PDOS, Bader charges, atomic magnetic moments, and O_2 structural features (see Table 2) comparing the data obtained on the reduced ATiO_2 (101) surfaces (with the VO1 O vacancy), in the presence or absence of coordinated *acac* and *dbm* ligands.

The analysis of the PDOS plot (Figure 3A) reveals that the adsorption of one O_2 molecule (low oxygen coverage) on the O-defective ATiO_2 (101) (VO1) surface in the absence of ligands creates states in the bandgap corresponding to i) the reduction of one Ti atom that traps in its d orbitals one of the two electrons left by the O vacancy (red peak) and ii) the transfer of the second electron from the surface to the π^* orbital of the oxygen molecule (orange peak below the Fermi level), which is reduced to a superoxide anion (O_2^-).^[31,40,42] Moreover, the observed

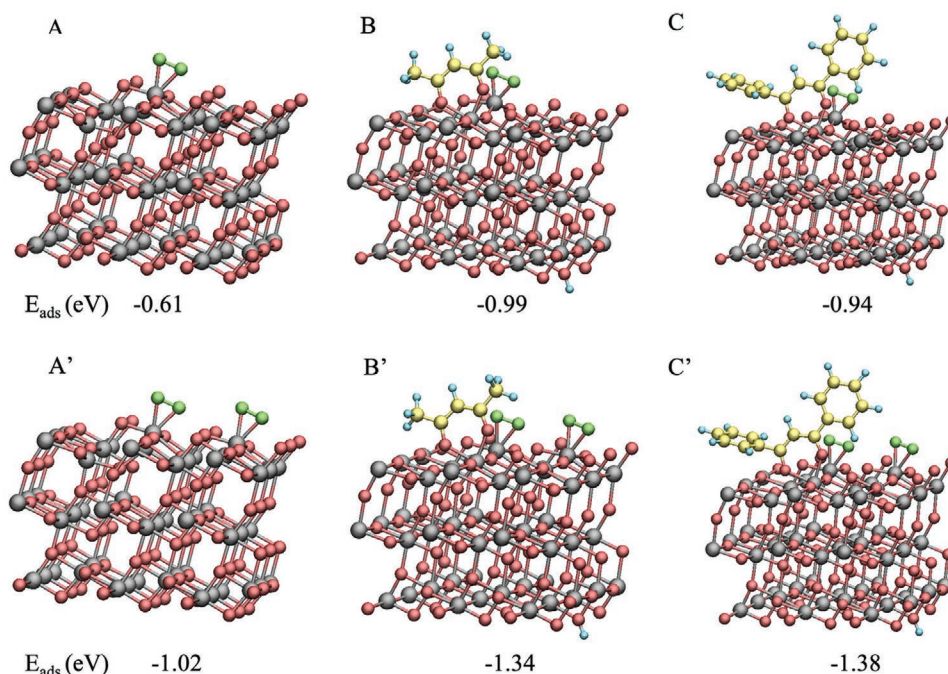


Figure 2. Optimized structures of one O₂ and two O₂ adsorption on VO1 surfaces A,A') in absence and in the presence of B,B') *acac* and C,C') *dbm* ligands with the corresponding E_{ads} in eV. Ti, C, H, O surface atoms and O₂ molecules are represented in ball and sticks, and depicted in gray, yellow, cyan, red, and green, respectively. The enlargements of the adsorption areas are shown in Figures S5 (Supporting Information).

O–O bond elongation to 1.33 Å (as compared with $d_{\text{O-O}}$ of 1.23 Å for O₂ gas phase) with an appreciable charge transfer from the surface and the retain of half of the original magnetic moment for each oxygen atoms (see Table 2) further confirm the formation of the superoxide anion.^[45–47]

Moving to the adsorption of two O₂ (high oxygen coverage), the PDOS (Figure 3B) shows bandgap states related to the transfer of the two electrons from the surface to the π^* orbital of each oxygen molecule (orange peak below the Fermi level).^[31,40,42] Therefore, the formation of two superoxide anions and simultaneously the oxidation of two Ti³⁺ to Ti⁴⁺ is observed. Moreover, this interpretation is also confirmed by the results reported in Table 2 and by bonding charge analysis (Figure S8, Supporting Information), indicating how the charge distributes on both O₂ molecules during the reduction process. In both cases, the PDOS plots display a bandgap state above the Fermi level (0 eV) corresponding to the empty $\sigma 2p^*$ orbital of the O₂ molecule(s).

Table 1. Adsorption energies (E_{ads} , eV) of one O₂ and two O₂ molecules on VO1 surface in the presence of *acac* and *dbm*, and total energy gain (E_{tot}) related to VO1 formation, coordination of ligand, and adsorption of one/two O₂ molecules.

E_{ads} [eV]	<i>acac</i>	<i>dbm</i>
O ₂ on (VO1+ligand)	–0.99	–0.94
2O ₂ on (VO1+ligand)	–1.34	–1.38
E_{tot} (O ₂ , VO1)	–0.45	–0.45
E_{tot} (2O ₂ , VO1)	–0.79	–0.88

Concerning the adsorption of oxygen molecules on VO1+*acac/dbm* surfaces, a key effect of the O₂ coverage emerges; the formation of a peroxide anion is observed when only one oxygen molecule is considered (Figure 4A,B), while superoxide anions form in the presence of two O₂ adsorbed on the surface (Figure 4C,D). In all cases, the electron transfer from the surface to the O₂ molecule(s) is observed (see the corresponding spin density analysis in Figure 4 and the Bader charges and magnetic moment on each oxygen atom (μ_{O}) of O₂ molecule(s) in Table 2).

In detail, for both ligands, at low oxygen coverage, the PDOS plots do not have bandgap states above the Fermi level, most likely since the peroxide anions are generated by transferring two electrons from the surface to the π^* and $\sigma 2p^*$ orbitals of

Table 2. O–O equilibrium distance ($d_{\text{O-O}}$), Bader charges variations calculated with respect to the charge of O₂ in gas phase (Δq_{O_2}), atomic magnetic moment on each oxygen atom (μ_{O}) of O₂ molecules in gas phase and upon adsorption on VO1 and VO1+*acac/dbm* surfaces.

O ₂	O ₂ (free)	VO1	VO1+ <i>acac</i>	VO1+ <i>dbm</i>
$d_{\text{O-O}}$ [Å]	1.23	1.33	1.46	1.46
Δq_{O_2} [e [–]]	0.00	0.49	0.97	0.94
$ \mu_{\text{O}1} \mu_{\text{O}2} [\mu]$	1.0 1.0	0.5 0.6	0.1 0.1	0.1 0.1
2O ₂				
$d_{\text{O-O}}$ [Å]	1.23–1.23	1.33–1.33	1.33–1.33	1.33–1.33
Δq_{O_2} [e [–]]	0.00–0.00	0.47–0.48	0.52–0.50	0.49–0.52
$ \mu_{\text{O}1} \mu_{\text{O}2} [\mu]$	1.0 1.0	0.6 0.5	0.5 0.5	0.6 0.5
	1.0 1.0	0.6 0.5	0.5 0.5	0.6 0.5

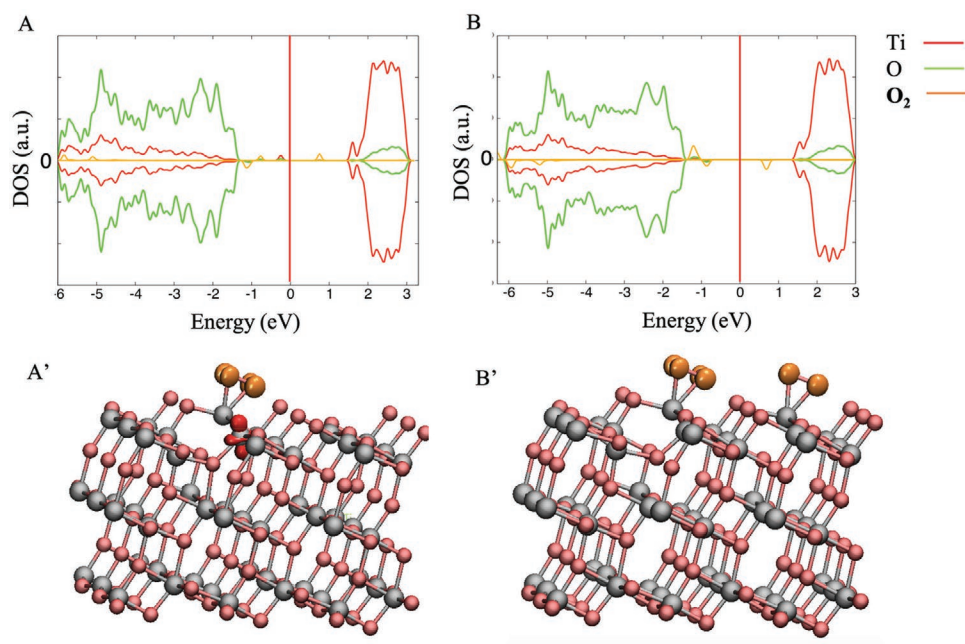


Figure 3. PDOS and spin density plot for relaxed structures of A,A') VO1+O₂ and B,B') VO1+2O₂. The state of titanium (Ti) and oxygen (O) surface atoms, and oxygen molecules (O₂) are represented in ball and sticks, and depicted in red, green, and orange, respectively. On the DOS (a.u.) axis, the values above and below 0 a.u. indicate the electrons with spin up and spin down, respectively. The Fermi energy level is represented with a red line at 0 eV.

the O₂. Consistently, the d_{O-O} increases to 1.46 Å and the magnetic moment reduces to |0.1| for each oxygen atom.

In contrast, moving to “high oxygen coverage,” the PDOS plots indicate the presence of bandgap states above the Fermi level, corresponding to the empty orbital $\sigma 2p^*$ of the O₂ molecules. Therefore, it is assumed that the superoxide anions are formed from the transfer of the two electrons from the surface to the π^* orbital of each oxygen molecule.^[31,40,42] The consequent formation of two superoxide anions is also confirmed by the O–O distance (1.33 Å), the Bader charges and the magnetic moments of the O₂ molecules (about |0.5|) reported in Table 2. The bonding charge analysis for two different oxygen coverages in the presence of *acac* and *dbm* is reported in Figure S9 (Supporting Information).

Consequently to the oxygen adsorption, a reduction of the bandgap occurs (values between 2.50 and 3.00 eV; see Table S5 in the Supporting Information). By combining the electronic analysis with the energetic results for all systems considered, it clearly emerges that the binding of β -diketones on the O-defective ATiO₂ raises the charge and traps it on the external layer of the surface, increasing the charge transfer to the adsorbed O₂. This strengthens the oxygen adsorption and, in turn, the stability of the whole system increases. In fact, at “low oxygen coverage,” for VO1 naked surface, only one of the two electrons in excess is transferred to the O₂ molecule with formation of a superoxide anion. In the presence of *acac* or *dbm* ligands, two electrons are driven from the surface to the O₂ molecule with the formation of a peroxide anion. As a result, E_{ads} of a single O₂ in the absence of ligand is about half than the E_{ads} calculated in the presence of *acac* or *dbm*. At “high oxygen coverage,” the ligands favor the adsorption also of the second O₂

molecule driving one electron to each oxygen molecule. As a consequence, the formation of the two superoxide anions on the surface is favored by 0.34 and 0.43 eV when *acac* and *dbm* are adsorbed, respectively. In Scheme 2, the proposed mechanism for the ROS formation in the presence of both ligands is reported.

2.3. Interaction of Catecholate Anion and Adsorption of O₂ Molecules on O-Defective Anatase TiO₂ (101) Surface

To test the mechanism proposed above, calculations on O-defective ATiO₂ (101) surface in the presence of catechol (H₂*cat*) as a ligand were performed. Upon adsorption on the anatase surface, H₂*cat* deprotonates and, also in this case, the two protons (H⁺) resulting from the dissociation are put on O2c sites of the bottom layer of the slab far from the molecule. The most stable geometry related to the interaction between catecholate anion (*cat*) and VO1 surface shows the ligand bound to the surface by means of a bidentate coordination (B), in which two oxygens coordinate a Ti4c (Ti1) and one oxygen a Ti5c (Ti2) restoring the hexa-coordination of both unsaturated Ti atoms derived from vacancy formation (Figure 5A and Scheme 3).^[48,49] Consistent with the presence of two negative charges for *cat*, its interaction with the surface induces a charge transfer to the surface that is double than that observed for *dbm* and *acac* ligand ($\Delta q = -0.88$; Table S6, Supporting Information). However, E_{int} results in 0.43–0.58 eV less favored than that for the two diketones (compare to E_{int} reported in Figure 5A with the values reported in Figure 1A,B for *acac* and *dbm*, respectively). Moreover, the formation of the ROS at low and high oxygen coverages (Figure 5B,C),

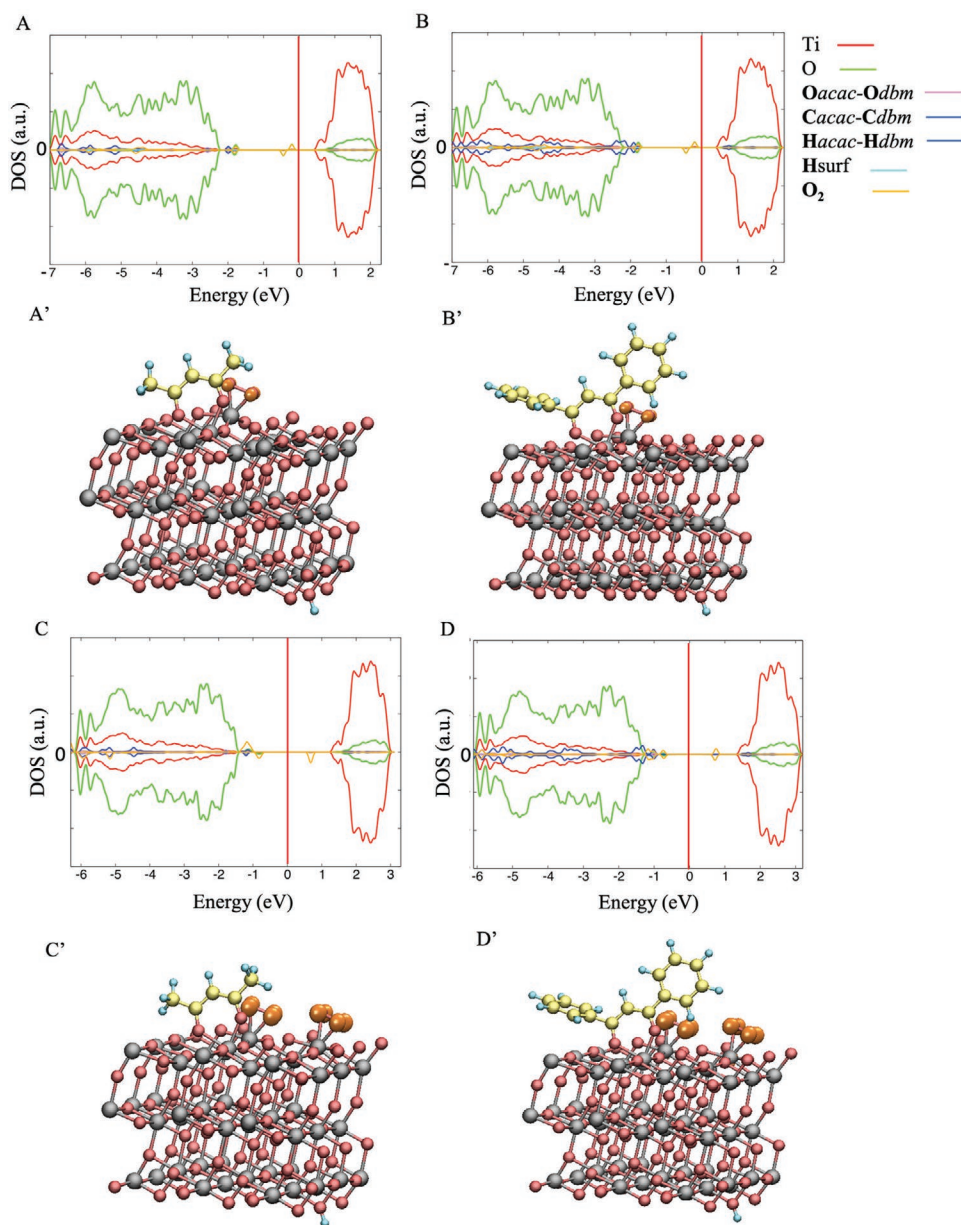
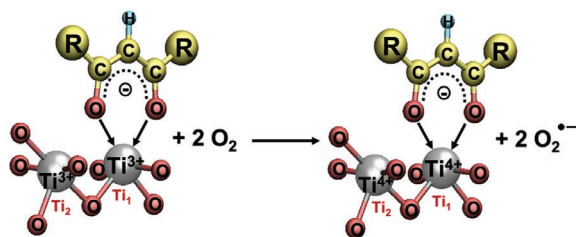


Figure 4. PDOS and spin density plot for relaxed structures A,A',B,B') *acac/dbm-VO1+O₂* and C,C',D,D') *acac/dbm-VO1+2O₂*. The state of titanium (Ti) and oxygen (O) surface atoms, and oxygen (*Oacac*, *Odbm*), carbon (*Cacac*, *Cdbm*), and hydrogen (*Hacac*, *Hdbm*) ligand atoms, surface hydrogen (*Hsurf*), and oxygen molecules (*O₂*) are represented in red, green, pink, blue, cyan, and orange, respectively. On the DOS (a.u.) axis, the values above and below 0 a.u. indicate the electrons with spin up and spin down, respectively. The Fermi energy level is represented with a red line at 0 eV.



Scheme 2. Mechanism for the formation of superoxide anions on *ATiO₂* surface with coordinated diketonate ligands. Ti, C, H, and O atoms are represented in ball and sticks and depicted in gray, yellow, cyan, and red, respectively.

respectively, calculated from the starting stoichiometric surface (E_{tot}), becomes even endergonic in the presence of *cat* (see last two rows in Table 3). The same calculations performed on the stoichiometric surface are reported in Section S3 of the Supporting Information.

Looking at the electronic variation at the surface, the PDOS and the spin density plots of *cat-VO1* (Figure 6A,A') reveal that the excess of electrons within the surface localizes in the d orbitals of the Ti atoms far from the vacancy and deep into the subsurface layers. As a consequence, the external layer of the surface is less charged and the adsorption of the oxygen is less

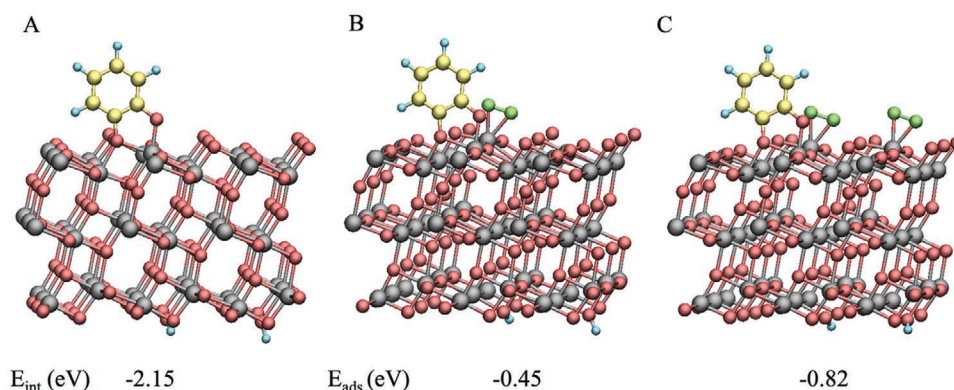


Figure 5. Optimized structures of A) *cat*, B) O_2 , and C) 2O_2 adsorbed on VO1 surface with the corresponding E_{int} (eV) and E_{ads} (eV). Ti, C, H, O atoms, and O_2 molecules are represented in ball and sticks and depicted in gray, yellow, cyan, red, and green, respectively. The enlargements of the adsorption areas are shown in Figures S5 (Supporting Information).

avored by 0.54–0.49 eV for each O_2 molecule adsorbed when compared with the corresponding results obtained with *acac* and *dbm* (Table 1).

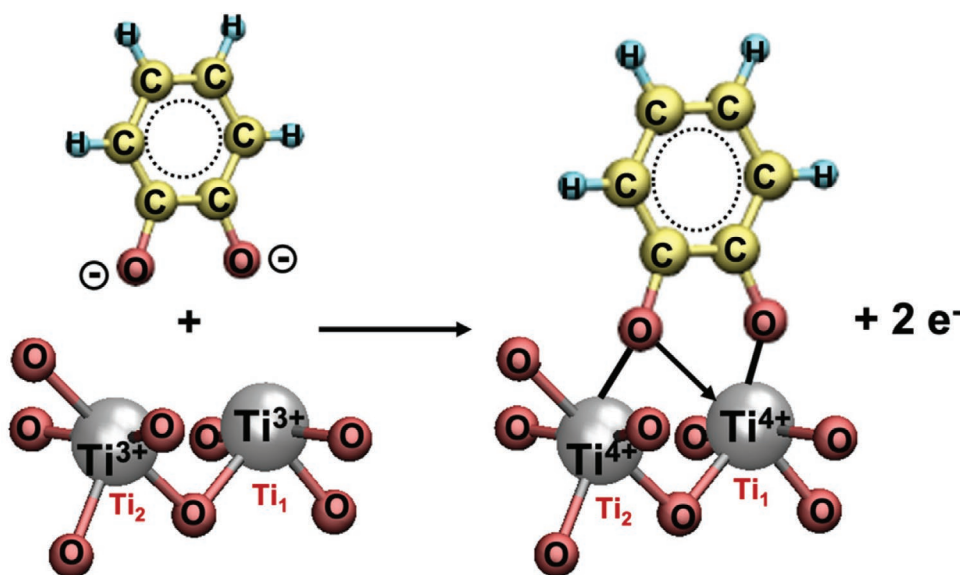
In conclusion, although Bader charges and structural analysis of the oxygen molecules on the surface (Table 4) together with the corresponding PDOS and spin density analysis indicate the formation of superoxide anions at both low and high oxygen coverages (Figure 6B,B' and Figure 6C,C', respectively), intriguingly the calculated stability of the resulting surfaces turns out as low as observed for VO1 surface in the absence of ligand. Accordingly, for a bare amorphous TiO_2 , the formation of the ROS is not experimentally observed,^[29] as for the interaction of *cat* with the surface (see the following section).

Based on our mechanism and according to all results herein reported, catechol is not able to trap the excess of charge generated by vacancy formation due to an ineffective

delocalization of the electrons in the binding site contrary to the case of *acac* and *dbm* (Schemes 2 and 3). In contrast, the interaction of catechol with the surface induces the oxidation of two Ti^{3+} to Ti^{4+} releasing an excess of charge that distributes on the entire surface. Due to a decrease of the charge localization nearby the vacancy, the oxygen adsorption is less favored, and thus the consequent superoxide anions are less stable, in agreement with experimental results reported in the following.

2.4. DFT HOMO–LUMO Analysis of Neutral Ligands and of VO1 + Ligand Surfaces

From the results discussed so far, it emerges that the main role played by the ligands in the ROS formation and stabilization is to increase the excess of charge on the VO1 surface and to drive



Scheme 3. Interaction between catechololate anion (*cat*) and O-defective ATiO_2 surface. Ti, C, H, and O atoms are represented in ball and sticks and depicted in gray, yellow, cyan, and red, respectively.

Table 3. Adsorption energies (E_{ads} , eV) of O_2 molecule(s) on VO1 surface in the presence of *cat* and total energy gain (E_{tot}) related to VO1 formation, coordination of *cat* ligand, and adsorption of one/two O_2 .

E_{ads} [eV]	<i>cat</i>
O_2 on (VO1+ <i>cat</i>)	-0.45
2O_2 on (VO1+ <i>cat</i>)	-0.82
E_{tot} (O_2 , VO1)	0.53
E_{tot} (2O_2 , VO1)	0.15

it into the external layer stabilizing the Ti^{3+} species formed as result of the O-vacancies. For a deeper understanding of the electronic features of the ligands that can explain the different behavior in the ROS formation and stabilization, the HOMO and LUMO orbitals of the three organic ligands, free (*Hacac*, *Hdbm*, and H_2cat) and bonded to the VO1 surface (VO1+*acac/dbm/cat*), have been studied.

LUMO values of each free ligand, reported considering as reference the HOMO energy, show that *Hacac* and *Hdbm* have LUMO energies (3.29 and 2.31 eV, respectively) that are lower in energies of about 0.83 and 1.81 eV than that of H_2cat (4.12 eV), respectively.

Moreover, the plots of the HOMO and LUMO orbitals (see Figure S12 in the Supporting Information) show that, in the case of diketone species, the LUMO is localized on the dicarbonyl portion, while for H_2cat on the aromatic ring, that is far from the atoms directly involved in the interaction with VO1 surface. In conclusion, all the results indicate a greater accessibility of the LUMO orbitals in the case of *Hacac* and *Hdbm*, which accounts for the greater tendency of these ligands to trap

the electronic charge on the upper layer of the VO1 ATiO_2 (101) surface. In fact, moving to the analyses of the ligand bonded to the surface, in VO1+*acac/dbm*, HOMO and LUMO are localized on the Ti atoms of anatase (101) (Figure S13a,b, Supporting Information), while in VO1+*cat* (Figure S13c, Supporting Information) the HOMO is localized on the surface but the LUMO is on the organic ligand. As a consequence, in the presence of catechol, the formation of stable superoxides is not favored because of the tendency of the surface to move its electrons toward the LUMO of the ligand and not toward the adsorbed O_2 molecules, in agreement with experiments.

2.5. Synthesis and Physicochemical Characterization of TiO_2 -*acac*, TiO_2 -*dbm*, and TiO_2 -*cat* Hybrid Materials

In order to verify and validate the computational results, we have prepared and characterized samples of the three systems under investigation. The sol-gel route established for the synthesis of TiO_2 -*acac* hybrid materials, based on the complexation of Ti^{4+} ions by the organic ligand before hydrolysis and condensation reactions,^[29] has been applied also with dibenzoylmethane and catechol. Since the molecular structure and properties of the ligand strongly affect the reactivity of the modified titanium alkoxide precursor, and thus the evolution of the sol-gel process, each system requires an optimization of the synthesis conditions to give a homogeneous product with the desired characteristics. By the procedures described in Section S5 (Supporting Information) we obtained a chemical gel (TiO_2 -*acac*), a particulate gel (TiO_2 -*dbm*), and a physical gel (TiO_2 -*cat*) with the same nominal ligand/Ti molar ratio, equal

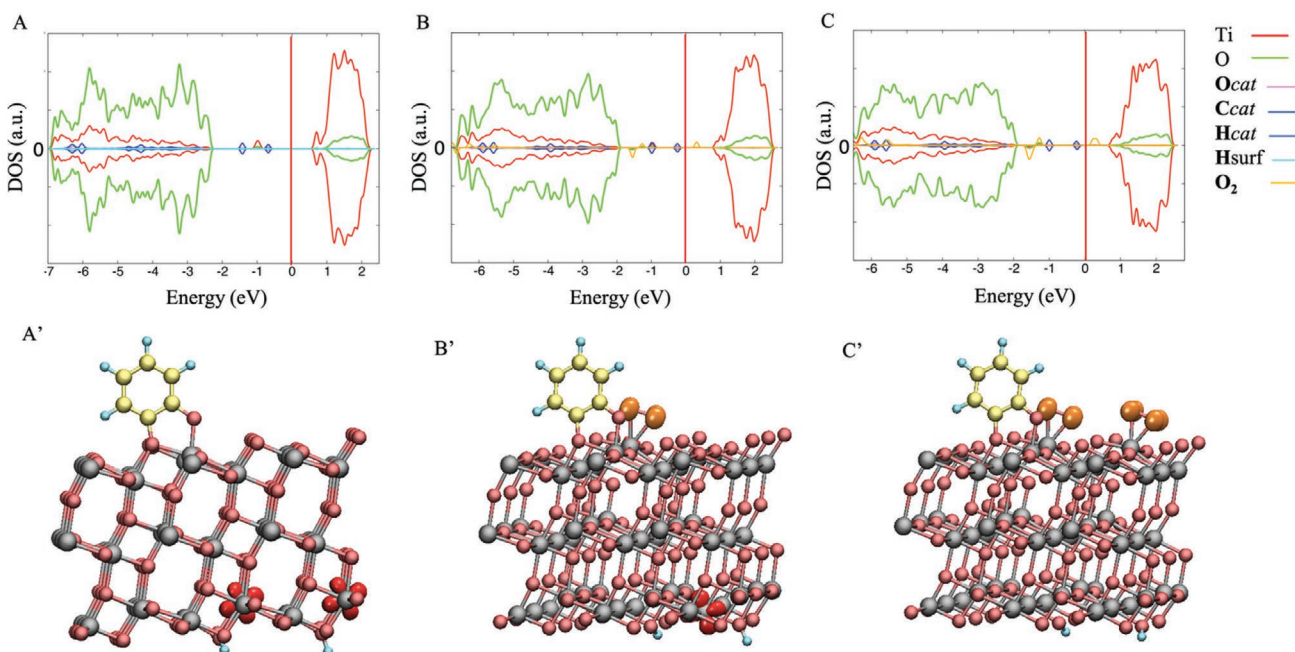


Figure 6. PDOS and spin density plot for relaxed structures of A,A') VO1+*cat*, B,B') VO1+*cat*+ O_2 , and C,C') VO1+*cat*+ 2O_2 . The state of titanium (Ti) and oxygen (O) surface atoms, oxygen (*Ocat*), carbon (*Ccat*), and hydrogen (*Hcat*) ligand atoms, surface hydrogen (*Hsurf*), and oxygen molecules (O_2) are represented in red, green, pink, blue, cyan, and orange, respectively. On the DOS (a.u.) axis, the values above and below 0 a.u. indicate the electrons with spin up and spin down, respectively. The Fermi energy level is represented with a red line at 0 eV.

Table 4. O–O equilibrium distance (d_{O-O}), Bader charge variations calculated with respect to the charge of O_2 in gas phase (Δq_{O_2}), atomic magnetic moment on each oxygen atom (μ_{O}) of O_2 molecules in gas phase and upon adsorption on $VO1+cat$ surface.

	$VO1+cat$ O_2	$VO1+cat$ $2O_2$
d_{O-O} [Å]	1.33	1.33–1.34
Δq_{O_2} [e ⁻]	0.50	0.50–0.51
$ \mu_{O1} $ $ \mu_{O2} $ [μ]	0.5 0.5	0.5 0.5 0.5 0.5

to 0.2. The dried gel samples are shown in Figure S14 (Supporting Information).

The samples have an amorphous structure, as expected for gel-derived materials heat-treated at low temperature.^[50,51] The organic components and their binding to the oxide matrix were investigated by Fourier-transform infrared (FTIR) spectroscopy (Figure 7A). All the samples present the bands characteristic of Ti–O–Ti vibrations below 800 cm^{-1} , the broad O–H stretching band above 3000 cm^{-1} , indicating a significant surface hydroxylation, and C–H stretching bands between 2850 and 3000 cm^{-1} , mainly due to residual alkoxide and alcohol molecules. The spectrum of TiO_2-acac closely resembles that previously reported for an analog with starting $acac/Ti$ molar ratio = 0.4.^[29] The two bands at 1580 and 1430 cm^{-1} are attributed to the asymmetric and symmetric stretching of the carbonyl groups coordinated to Ti^{4+} ions in the enolate form, and are compatible with a bidentate chelating mode, resulting slightly shifted to higher frequencies compared to those predicted for the $Ti(acac)_3$ complex.^[52] This is supported by the absence of bands around 1700 cm^{-1} , indicating the absence of free keto groups. The band at 1530 cm^{-1} can be assigned to C=C stretching coupled with C=CH bending, although some uncertainty arises in the literature,^[53] while the bands at 1360 and 1284 cm^{-1} should be due to C–O stretching and a combination of stretching modes, respectively.^[52]

$Hdbm$ is supposed to show a similar coordination as $Hacac$. The attribution of the most relevant features in the TiO_2-dbm FTIR spectrum follows that of TiO_2-acac ; in particular, the bands between 1593 and 1480 cm^{-1} should correspond to symmetric and asymmetric stretching of the coordinating carbonyl groups, and the band at 1360 cm^{-1} , not found in free $Hdbm$,^[54] can be assigned to a stretching of a C–O bond involved in the complexation, analogous to TiO_2-acac .^[34] Therefore, for both diketones, the chelate bidentate binding seems to be the prevalent geometry, in line with the computational results on the O-defective $ATiO_2$ (101) surface (Section 2.1).

The FTIR spectrum of TiO_2-cat presents two strong bands at 1479 and 1256 cm^{-1} , ascribed, respectively, to the stretching of the aromatic C–C bonds and of coordinating C–O groups, according to studies of catechol– TiO_2 interaction, which report similar spectral features.^[22,55] The coordination geometry of cat on TiO_2 is a debated aspect: some authors suggest that the chelating predominates,^[22,48,55,56] while others consider the bridging favored.^[57–59] The prevailing geometry may depend on the ligand surface coverage, the crystalline facet, and the adsorption sites,^[58] and its identification on the basis of vibrational spectra is not straightforward. The wavenumbers of the main bands observed in Figure 7A seem close to those measured for

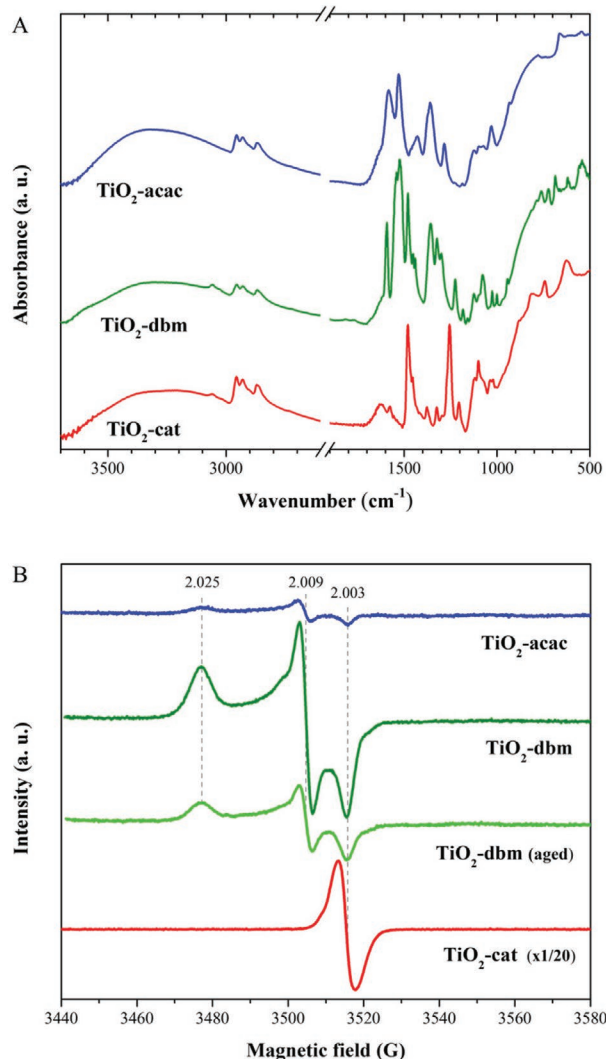


Figure 7. A) Fourier-transform Infrared (FTIR) spectra of the dried gels and B) electron paramagnetic resonance (EPR) spectra recorded at room temperature on the samples after the synthesis and on TiO_2-dbm also after 8 months (aged). The g values of the main EPR peaks are reported.

the $Ti(cat)_3^{2-}$ complex^[55] and intermediate between those predicted for bridging and chelating TiO_2-cat complexes.^[59] In our case, the complex is formed on the $Ti(IV)$ alkoxide precursor in the first stage of the synthesis procedure, so an initial chelating binding is expected. Despite its stability, during hydrolysis and condensation a distribution of binding modes may appear, including the one resulting the most stable on O-defective $ATiO_2$ (101) surface (Figure 5 and Scheme 3). Moreover, adsorbed catecholate was shown to have mobility across some TiO_2 surfaces, favored by an abundance of surface hydroxyls.^[57]

The occurrence of LMCT in the synthesized materials is confirmed by their optical properties. While neither TiO_2 nor the organic molecules alone absorb visible light, the hybrid samples have an intense coloration (yellow with diketones, dark brown with catechol; Figure S14, Supporting Information). Accordingly, the UV–vis–NIR diffuse reflectance spectra (Figure S15A, Supporting Information) of TiO_2-acac and TiO_2-dbm show

an absorption edge around 500 nm, whereas that of TiO₂-*cat* shows a larger redshift and a tail spreading in the NIR range. The apparent bandgaps resulting from the charge transfer complexes are evaluated by the Tauc plot (Figure S15B, Supporting Information) as about 2.6 eV for TiO₂-*acac*, 2.5 eV for TiO₂-*dbm* (in good accordance with the calculated values, 2.7 eV; see Figure 1A,B), and 2.0 eV for TiO₂-*cat*. The large band tail of the latter sample suggests a wide distribution of surface electron states, possibly related to a variety of *cat*-surface interaction modes. Studies on *cat*-modified TiO₂ usually reported an absorption band at around 420 nm, associated with the direct charge transfer from the π orbital (HOMO) of the molecule to Ti 3d orbitals.^[60,61] In concerned diketones, UV-vis spectra similar to ours were reported for *acac*-functionalized TiO₂ nanoparticles^[20] and thin films containing *dbm*.^[34] Although the additional absorption band in Ti-diketonate complexes has been often attributed to intraligand $\pi \rightarrow \pi^*$ transition, an interaction with the Ti 3d orbitals involving a partial LMCT character undoubtedly occurs also for these compounds, in agreement with our present calculations and with our previous hypothesis.^[29]

The most intriguing feature of the studied hybrid materials is enlightened by electron paramagnetic resonance (EPR) spectroscopy. The spectra (Figure 7B) were acquired on the dried samples at room temperature, in the dark, without any activation treatment. An amorphous bare TiO₂ sample, prepared by sol-gel without the addition of organic ligands, does not show any paramagnetic signal.^[21] TiO₂-*dbm* reveals a three-component anisotropic signal, analogous to that of TiO₂-*acac*^[29,32] and typical for the superoxide radical anion adsorbed on the surface of TiO₂.^[25] However, the TiO₂-*dbm* signal is distinguished by a strikingly higher intensity, corresponding to an estimated concentration of radicals of about $2 \times 10^{16} \text{ g}^{-1}$, one order of magnitude larger than that estimated for TiO₂-*acac* ($2 \times 10^{15} \text{ g}^{-1}$). Besides possible differences between the two samples, regarding particle size, surface area, and surface density of ligand, this result indicates that *dbm* is more efficient than *acac* in the generation of stable superoxide anions on the hybrid TiO₂ surface. The EPR measurements were performed about 1 month after the synthesis of the materials. For TiO₂-*acac* samples, the long-lasting persistence of the O₂⁻ signal was previously observed, up to 3 years, depending on the storage conditions, and the possible regeneration of the depleted radicals by mere contact with air was demonstrated.^[32] The TiO₂-*dbm* powder was analyzed again by EPR after storing it for 8 months in a test tube under ambient conditions. The signal (Figure 7B) was still well defined, though its intensity had decreased to about 1/3 of the initial value (corresponding to 7×10^{15} radicals g^{-1}). These results confirm the impressive capacity of these hybrid materials to maintain firmly adsorbed and likely to continuously generate superoxide anions on their surfaces and point at TiO₂-*dbm* as a very promising system.

On the other hand, TiO₂-*cat* shows a completely different EPR signal, a rather symmetric intense singlet centered at $g = 2.003$, and no trace of O₂⁻. A comparable spectrum, a broad singlet with $g = 2.0038$, was reported for TiO₂ nanoparticles with adsorbed catechol, analyzed at 4 K under visible light irradiation, and was assigned to the hole localized on the aromatic ring of the ligand after photoinduced charge transfer.^[22]

A similar signal, with $g = 2.0033$, was reported for a TiO₂ film surface modified with catechol, after an activation through a cyclic voltammetry scan, which oxidized *cat* to a stable semiquinone radical anion.^[19] The attribution of the observed EPR peak to an unpaired electron localized on the aromatic ring following LMCT is therefore reasonable. The very high intensity of the observed signal (about 2×10^{17} spin g^{-1}) and its persistence in the absence of light or other external stimuli point at an effective charge separation in the gel-derived TiO₂-*cat* material.

In summary, the experimental data on amorphous hybrid samples confirm the deep differences between the complexes formed in TiO₂-diketonate and TiO₂-*cat* systems, in excellent agreement with the DFT results on O-defective anatase TiO₂. *Cat* seems indeed more efficient in the LMCT, owing to a strong electronic coupling with TiO₂; however, it does not allow the remarkable stabilization of adsorbed superoxide radicals exhibited by *acac* and in particular by *dbm*.

3. Conclusion

In this work, the role played by the metal, by the structural features of the surface and of the ligand on the virtuous mechanism of formation and stabilization of superoxide radicals, for hybrid O-deficient anatase TiO₂ (101) surfaces is revealed by means of a synergistic theoretical and experimental approach.

From our study it emerges that the best composition of metal-oxide-based nanomaterials toward a stable and spontaneous production of ROS on the surface should include 1) reducible metal oxides, e.g., Ti(IV)/Ti(III), 2) superficial oxygen vacancies which leave electrons and Ti³⁺ coordinatively unsaturated on the surface, 3) organic ligands that transfer charge on the surface by binding to a single Ti³⁺ and characterized by a low LUMO energy driving the excess of the charge on the external surface close to the reduced metal ions.

As a result, the bidentate binding of a β -diketone ligand, as acetylacetone and dibenzoylmethane, on the O-defective TiO₂ reduces the bandgap of the system and increases the charge on the surface that is trapped on the external layer in proximity of the Ti³⁺ ions. This localized excess of charge strengthens the oxygen adsorption and increases both the stability of the whole system and the charge transfer to the adsorbed O₂, leading to an easy formation of spontaneous ultrastable ROS species, in agreement with experiments.

As a further support of our finding, in the presence of catechol as a ligand, the formation of ROS becomes endothermic and experimentally is not observed.

The concept and the practical improvement obtained from these studies will guide the design and manufacturing of tailored nanostructured metal oxide surfaces suitable for specific applications and the improvement of their efficiency in different fields, among which reduction of water/air pollution, disinfection, and self-cleaning coatings even in the absence of light irradiation. In addition, the application of our insights may promote the implementation of related nanotechnologies to advance the development of photo-electrochemical systems for solar energy harvesting and photocatalytic materials for new environmental, medical, and sensing applications.

4. Computational Details

The calculations reported are based on the DFT and have been performed with the Quantum-ESPRESSO computer package.^[62] The exchange and correlation energy functional expressed in the Perdew–Burke–Ernzerhof (PBE) generalized gradient approximation (GGA)^[63] has been employed. The spin-polarized Kohn–Sham equations were solved in the plane-wave pseudopotential framework, with the wavefunction basis set and the Fourier representation of the charge density being limited by kinetic cutoffs of 25 and 250 Ry, respectively. The Ti, O, C, and H atoms were described by ultrasoft pseudopotentials.^[64]

We have used a DFT+*U* approach with a value of *U* = 3.9 eV, in line with other previous studies^[37,65,66] demonstrating that the addition of a Hubbard *U* term acting on the Ti 3d orbitals allows for a more accurate description of the electronic structure of titanium surfaces.^[37] Furthermore, to test our computational protocol, in the case of molecular oxygen adsorption, calculations with *U* values being lower (*U* = 3 eV) and higher (*U* = 5 eV) than 3.9 eV have been carried out, as suggested by the literature.^[40] The results of these tests indicate that Hubbard *U* term variation does not affect the formation of peroxide and superoxide anions.

For more details related to the models and experimental sections, see the Supporting Information.

Supporting Information

Supporting Information is available from the Wiley Online Library or from the author.

Acknowledgements

I.R. and C.I. contributed equally to this work. I.R. thanks MIUR and European Union for AIM-International Attraction and Mobility Call for Researchers funded by PON RI 2014–2020. The authors thank Prof. Gerardino D'Errico of the Department of Chemical Sciences of the University of Naples Federico II for providing the access to EPR instrument and for the help in EPR investigation. For computer time, this research used the resources of the KAUST Super-Computing Laboratory (KSL) at KAUST.

Conflict of Interest

The authors declare no conflict of interest.

Data Availability Statement

Research data are not shared.

Keywords

density functional calculations, hybrid materials, O₂ activation, sol–gel processes, superoxide radical anion

Received: April 16, 2021

Revised: June 14, 2021

Published online: August 8, 2021

- [1] S. Lacombe, T. Pigot, *Catal. Sci. Technol.* **2016**, *6*, 1571.
- [2] M. Hayyan, M. A. Hashim, I. N. AlNashef, *Chem. Rev.* **2016**, *116*, 3029.
- [3] Y. Nosaka, A. Y. Nosaka, *Chem. Rev.* **2017**, *117*, 11302.
- [4] W. Kim, T. Tachikawa, G. Moon, T. Majima, W. Choi, *Angew. Chem., Int. Ed. Engl.* **2014**, *53*, 14036.
- [5] M. Buchalska, M. Kobielski, A. Matuszek, M. Pacia, S. Wojtyła, W. Macyk, *ACS Catal.* **2015**, *5*, 7424.
- [6] D. K. Pallotti, L. Passoni, M. Maddalena, F. Di Fronzo, S. Lettieri, *J. Phys. Chem. C* **2017**, *121*, 9011.
- [7] Q. Chen, H. Wang, C. Wang, R. Guan, R. Duan, Y. Fang, X. Hiu, *Appl. Catal., B* **2020**, *262*, 118258.
- [8] S. M. Imani, L. Ladouceur, T. Marshall, R. Maclachlan, L. Soleymani, T. F. Didar, *ACS Nano* **2020**, *14*, 12341.
- [9] R. Nakano, H. Ishiguro, Y. Yao, J. Kajioaka, A. Fujishima, K. Sunada, M. Minoshima, K. Hashimoto, Y. Kubota, *Photochem. Photobiol. Sci.* **2012**, *11*, 1293.
- [10] B. Yang, Y. Chen, J. Shi, *Chem. Rev.* **2019**, *119*, 4881.
- [11] D. Chen, Q. Yu, X. Huang, H. Dai, T. Luo, J. Shao, P. Chen, J. Chen, W. Huang, X. Dong, *Small* **2020**, *16*, 2001059.
- [12] Z. Youssef, V. Jouan-Hureauux, L. Colombeau, P. Arnoux, A. Moussaron, F. Baros, J. Toufaily, T. Hamieh, T. Roques-Carnes, C. Frochet, *Photodiagn. Photodyn. Ther.* **2018**, *22*, 115.
- [13] N. Serpone, *J. Phys. Chem. B* **2006**, *110*, 24287.
- [14] S. G. Kumar, L. G. Devi, *J. Phys. Chem. A* **2011**, *115*, 13211.
- [15] M. Nolan, A. Iwaszuk, A. K. Lucid, J. J. Carey, M. Fronzi, *Adv. Mater.* **2016**, *28*, 5425.
- [16] H. Park, H. Kim, G. Moon, W. Choi, *Energy Environ. Sci.* **2016**, *9*, 411.
- [17] G. Zhang, G. Kim, W. Choi, *Energy Environ. Sci.* **2014**, *7*, 954.
- [18] G. Luciani, C. Imperato, G. Vitiello, *Catalysts* **2020**, *10*, 103.
- [19] Z. Tachan, I. Hod, A. Zaban, *Adv. Energy Mater.* **2014**, *4*, 1301249.
- [20] S. Varaganti, G. Ramakrishna, *J. Phys. Chem. C* **2010**, *114*, 13917.
- [21] A. Aronne, M. Fantauzzi, C. Imperato, D. Atzei, L. De Stefano, G. D'Errico, F. Sannino, I. Rea, D. Pirozzi, B. Elsener, P. Pernice, A. Rossi, *RSC Adv.* **2017**, *7*, 2373.
- [22] T. Rajh, L. X. Chen, K. Lukas, T. Liu, M. C. Thurnauer, D. M. Tiede, *J. Phys. Chem. B* **2002**, *106*, 10543.
- [23] M. Gerosa, C. E. Bottani, L. Caramella, G. Onida, C. Di Valentin, G. Pacchioni, *J. Chem. Phys.* **2015**, *143*, 134702.
- [24] C. Imperato, M. Fantauzzi, C. Passiu, I. Rea, C. Ricca, U. Aschauer, F. Sannino, G. D'Errico, L. De Stefano, A. Rossi, A. Aronne, *J. Phys. Chem. C* **2019**, *123*, 11581.
- [25] E. Carter, A. F. Carley, D. M. Murphy, *J. Phys. Chem. C* **2007**, *111*, 10630.
- [26] P. Lyu, J. Zhu, C. Han, L. Qiang, L. Zhang, B. Mei, J. He, X. Liu, Z. Bian, H. Li, *ACS Appl. Mater. Interfaces* **2021**, *13*, 2033.
- [27] D. Wang, L. Zhao, D. Wang, L. Yan, C. Jing, H. Zhang, L. Guo, N. Tang, *Phys. Chem. Chem. Phys.* **2018**, *20*, 18978.
- [28] J. Ragai, *Nature* **1987**, *325*, 703.
- [29] F. Sannino, P. Pernice, C. Imperato, A. Aronne, G. D'Errico, L. Minieri, M. Perfetti, D. Pirozzi, *RSC Adv.* **2015**, *5*, 93831.
- [30] F. Sannino, D. Pirozzi, G. Vitiello, G. D'Errico, A. Aronne, E. Fanelli, P. Pernice, *Appl. Catal., B* **2014**, *156–157*, 101.
- [31] A. B. Munoz-Garcia, F. Sannino, G. Vitiello, D. Pirozzi, L. Minieri, A. Aronne, P. Pernice, M. Pavone, G. D'Errico, *ACS Appl. Mater. Interfaces* **2015**, *7*, 21662.
- [32] D. Pirozzi, C. Imperato, G. D'Errico, G. Vitiello, A. Aronne, F. Sannino, *J. Hazard. Mater.* **2020**, *387*, 121716.
- [33] F. Sannino, P. Pernice, L. Minieri, G. A. Camandona, A. Aronne, D. Pirozzi, *ACS Appl. Mater. Interfaces* **2015**, *7*, 256.
- [34] a) H. Segawa, S. Adachi, Y. Arai, K. Yoshida, *J. Am. Ceram. Soc.* **2003**, *86*, 761; b) M. L. Addonizio, A. Aronne, C. Imperato, *Appl. Surf. Sci.* **2020**, *502*, 144095.

- [35] Up to now *dbm* has been employed as complexing agent of Ti^{4+} only for the synthesis of hybrid films.
- [36] A. Aronne, F. Sannino, S. R. Bonavolontà, E. Fanelli, A. Mingione, P. Pernice, *Environ. Sci. Technol.* **2012**, *46*, 1755.
- [37] M. Setvin, C. Franchini, X. Hao, M. Schmid, A. Janotti, M. Kaltak, C. G. Van de Walle, G. Kresse, U. Diebold, *Phys. Rev. Lett.* **2014**, *113*, 086402.
- [38] Y. He, O. Dulub, H. Cheng, A. Selloni, U. Diebold, *Phys. Rev. Lett.* **2009**, *102*, 106105.
- [39] H. Tang, H. Berger, P. E. Schmid, F. Lévy, G. Burri, *Solid State Commun.* **1993**, *87*, 847.
- [40] U. Aschauer, J. Chen, A. Selloni, *Phys. Chem. Chem. Phys.* **2010**, *12*, 12956.
- [41] The positions of the O_2 adsorbed on $Ti5c$ as close as possible to the surface O atom vacancy (VO1) were chosen based on literature data [38].
- [42] Y. F. Li, U. Aschauer, J. Chen, A. Selloni, *Acc. Chem. Res.* **2014**, *47*, 3361.
- [43] M. Setvin, J. Hulva, G. S. Parkinson, M. Schmid, U. Diebold, *Proc. Natl. Acad. Sci. USA* **2017**, *114*, E2556.
- [44] This is in line with the theoretical results performed on the $ATiO_2$ (101) with subsurface vacancies [38].
- [45] T. Berger, M. Sterrer, O. Diwald, E. Knozinger, D. Panayotov, T. L. Thompson, J. T. Yates, *J. Phys. Chem. B* **2005**, *109*, 6061.
- [46] D. Halwidl, W. Mayr-Schmolzer, M. Setvin, D. Fobes, J. Peng, Z. Mao, M. Schmid, F. Mittendorfer, J. Redinger, U. Diebold, *J. Mater. Chem. A* **2018**, *6*, 5703.
- [47] By taking into account O_2E_{ads} of -0.6 eV, our calculations are in qualitative agreement with the experimental results reported in the literature for the formation of superoxide anions on the O-defective vacancies surface of $ATiO_2$.
- [48] D. Finkelstein-Shapiro, S. K. Davidowski, P. B. Lee, C. Guo, G. P. Holland, T. Rajh, K. A. Gray, J. L. Yarger, M. Calatayud, *J. Phys. Chem. C* **2016**, *120*, 23625.
- [49] Y. Xu, W. K. Chen, S. H. Liu, M. J. Cao, J. Q. Li, *Chem. Phys.* **2007**, *331*, 275.
- [50] A. Aronne, E. Marenga, V. Califano, E. Fanelli, P. Pernice, M. Trifuoggi, A. Vergara, *J. Sol-Gel Sci. Technol.* **2007**, *43*, 193.
- [51] G. Bagnasco, C. Cammarano, M. Turco, S. Esposito, A. Aronne, P. Pernice, *Thermochim. Acta* **2008**, *471*, 51.
- [52] I. Diaz-Acosta, J. Baker, J. F. Hinton, P. Pulay, *Spectrochim. Acta, Part A* **2003**, *59*, 363.
- [53] T. A. Egerton, N. J. Everall, J. A. Mattinson, L. M. Kessel, I. R. Tooley, *J. Photochem. Photobiol., A* **2008**, *193*, 10.
- [54] S. F. Tayyari, H. Rahemi, A. R. Nekoei, M. Zahedi-Tabrizi, Y. A. Wang, *Spectrochim. Acta, Part A* **2007**, *66*, 394.
- [55] T. Lana-Villarreal, A. Rodes, J. M. Pérez, R. Gómez, *J. Am. Chem. Soc.* **2005**, *127*, 12601.
- [56] P. C. Redfern, P. Zapol, L. A. Curtiss, T. Rajh, M. C. Thurnauer, *J. Phys. Chem. B* **2003**, *107*, 11419.
- [57] S. C. Li, L.-N. Chu, X.-Q. Gong, U. Diebold, *Science* **2010**, *328*, 882.
- [58] S. C. Li, Y. Losovyj, U. Diebold, *Langmuir* **2011**, *27*, 8600.
- [59] T. D. Savić, M. I. Čomor, J. M. Nedeljković, D. Ž. Veljković, S. D. Zarić, V. M. Rakić, I. A. Janković, *Phys. Chem. Chem. Phys.* **2014**, *16*, 20796.
- [60] J. Moser, S. PUNCHIHewa, P. P. Infelta, M. Graetzel, *Langmuir* **1991**, *7*, 3012.
- [61] P. Persson, R. Bergström, S. Lunell, *J. Phys. Chem. B* **2000**, *104*, 10348.
- [62] P. Giannozzi, et al., *J. Phys.: Condens. Matter* **2017**, *29*, 465901.
- [63] J. P. Perdew, K. Burke, M. Ernzerhof, *Phys. Rev. Lett.* **1996**, *77*, 3865.
- [64] D. Vanderbilt, *Phys. Rev. B* **1990**, *41*, 7892.
- [65] M. Setvin, X. Shi, J. Hulva, T. Simschitz, G. S. Parkinson, M. Schmid, C. Di Valentin, A. Selloni, U. Diebold, *ACS Catal.* **2017**, *7*, 7081.
- [66] P. M. Kowalski, M. Farnesi Camellone, N. N. Nair, B. Meyer, D. Marx, *Phys. Rev. Lett.* **2010**, *105*, 146405.